Comprehensive proteome analysis of skeletal muscle in cachexia and age-related sarcopenia: a pilot comparison of in vivo and in vitro models

Ebhardt, H.Alexander; Degen, Simone ; Tadini, Valentina; Schilb, Alain; Johns, Neil ; Greig, Carolyn; Fearon, Kenneth CH; Aebersold, Ruedi; Jacobi, Carsten

DOI:
10.1002/jcsm.12188

ORIGINAL ARTICLE

Journal of Cachexia, Sarcopenia and Muscle (2017)
Published online in Wiley Online Library (wileyonlinelibrary.com) **DOI:** 10.1002/jcsm.12188

Comprehensive proteome analysis of human skeletal muscle in cachexia and sarcopenia: A pilot study

H. Alexander Ebhardt[1,6], Simone Degen[3], Valentina Tadini[3], Alain Schilb[3], Neil Johns[5], Carolyn A. Greig[4], Kenneth C.H. Fearon[5], Ruedi Aebersold[1,2] & Carsten Jacobi[3]*

[1]*Institute of Molecular Systems Biology, Department of Biology, ETH Zürich, Zürich, Switzerland;* [2]*Faculty of Science, University of Zürich, Zürich, Switzerland;* [3]*Novartis Institutes for BioMedical Research Basel, Novartis Pharma AG, Basel, Switzerland;* [4]*School of Sport, Exercise, and Rehabilitation Sciences and MRC-Arthritis Research UK Centre for Musculoskeletal Ageing Research, University of Birmingham, Birmingham, UK;* [5]*Clinical Sciences (Surgery), University of Edinburgh, Edinburgh, Scotland, UK;* [6]*Systems Biology Ireland, University College Dublin, Dublin, Ireland*

Abstract

Background Cancer cachexia (cancer-induced muscle wasting) is found in a subgroup of cancer patients leaving the patients with a poor prognosis for survival due to a lower tolerance of the chemotherapeutic drug. The cause of the muscle wasting in these patients is not fully understood, and no predictive biomarker exists to identify these patients early on. Skeletal muscle loss is an inevitable consequence of advancing age. As cancer frequently occurs in old age, identifying and differentiating the molecular mechanisms mediating muscle wasting in cancer cachexia vs. age-related sarcopenia are a challenge. However, the ability to distinguish between them is critical for early intervention, and simple measures of body weight may not be sufficiently sensitive to detect cachexia early.

Methods We used a range of omics approaches: (i) undepleted proteome was quantified using advanced high mass accuracy mass spectrometers in SWATH-MS acquisition mode; (ii) phospho epitopes were quantified using protein arrays; and (iii) morphology was assessed using fluorescent microscopy.

Results We quantified the soluble proteome of muscle biopsies from cancer cachexia patients and compared them with cohorts of cancer patients and healthy individuals with and without age-related muscle loss (aka age-related sarcopenia). Comparing the proteomes of these cohorts, we quantified changes in muscle contractile myosins and energy metabolism allowing for a clear identification of cachexia patients. In an *in vitro* time lapse experiment, we mimicked cancer cachexia and identified signal transduction pathways governing cell fusion to play a pivotal role in preventing muscle regeneration.

Conclusions The work presented here lays the foundation for further understanding of muscle wasting diseases and holds the promise of overcoming ambiguous weight loss as a measure for defining cachexia to be replaced by a precise protein signature.

Keywords Cancer cachexia; Proteome quantification; SWATH-MS; Signal transduction; TNFα

Received: 5 October 2016; Revised: 3 January 2017; Accepted: 10 January 2017
**Correspondence to: Carsten Jacobi, Novartis Institutes for BioMedical Research Basel, Novartis Pharma AG, Basel, Switzerland. Phone: +41795092595, Email:* carsten.jacobi@novartis.com

Introduction

Skeletal muscle develops from mono-nucleated myoblasts into multi-nucleated myotubes which then mature into myofibres, a process termed myogenesis.[1] Once development is complete, skeletal muscles are essential for locomotion and respiration.[2] Beyond the obvious role in locomotion, skeletal muscle is a metabolically important organ for glucose uptake and storage and a reservoir for amino acids.[3] As such, it is not surprising that metabolic diseases such as type II diabetes can alter the composition of muscle tissue.[4] Skeletal muscle is plastic and responds to use (and disuse), ageing, and disease. In elderly people, several of these conditions may co-exist, and the cause of

muscle wasting could not easily be allocated to a single condition. Hence, a molecular description of these different groups may hold the key to unequivocally differentiate between normal age-related muscle loss and chronic disease-related muscle wasting.[5–7] Weight loss and muscle wasting as a result of chronic disease such as cancer, heart failure, renal failure, or chronic obstructive pulmonary disease is termed cachexia.[8] Currently, it is challenging to differentiate between muscle loss due to age-related sarcopenia or cachexia, but distinguishing them is critical for early intervention.[9] The most common method used in clinics to differentiate modes of muscle loss is body weight measurement over six months in combination with muscle strength assessment.[10,11] Despite weight stability, skeletal muscle loss can still occur in elderly people.[12] Hence, a more specialized current clinical assessment of muscle utilizes dual energy X-ray absorptiometry (DXA) scans to obtain accurate measurement of muscle mass. A DXA scan in combination with height measurements is used to calculate a relative skeletal muscle index (RSMI).

Identification of the underlying molecular mechanisms involved in cancer cachexia (cca) remains elusive. It may possibly be that different mechanisms causing cca may require different therapeutic approaches. In light of technological advancements, omics and systems biology approaches have started to shine light onto the molecular pathology of muscle-related diseases.[13] The main analytical challenge for proteomics as an unbiased tool for protein quantification is the composition of muscle tissue itself. Global protein identification and quantification are limited due to the high number of contractile muscle proteins that make the analysis of low abundant proteins challenging. Further, structural proteins are frequently homologous in terms of protein sequence, allowing only quantitative statements about protein groups. In addition, a high number of contractile muscle proteins lead to an ion suppression effect thus masking underlying signaling proteins.[14]

In the past, proteomic studies of skeletal muscle included 1D or 2D peptide separation in combination with cation exchange chromatography and liquid chromatography coupled to tandem mass spectrometer (LC–MS/MS) to generate a catalogue of proteins identifiable in human muscle biopsies.[15,16] Advances in analytical technologies allowed for the expansion of the detectable proteome in both animal biopsies and cell line models.[17] By isolating single mouse muscle fibres, Murgia and co-workers were able to quantify proteomes specific to fast or slow muscles revealing an unexpected muscle type specific mitochondrial adaptation.[18] Other proteomic studies investigated the plasticity of the muscle tissue proteome from human biopsies over a variety of clinically observed situations. Brocca and colleagues quantified proteome changes due to disuse using 2D electrophoresis and found myofibrillar proteins, metabolic enzymes, and antioxidant defense systems down-regulated after 35 days of bed rest.[19] Staunton and coworkers characterized proteome changes due to age-dependent muscle loss and detected changes in muscle metabolism, ion handling, and the cellular stress response as a function of aging.[20] Besides physical and age-dependent proteome changes, genetic diseases also perturb the normal proteome in muscles.[21] Doran and colleagues investigated the effects of the inheritable neuromuscular disorder Duchenne muscular dystrophy using 2D gel electrophoresis and identified 35 at least two-fold differentially regulated proteins comparing a normal with a dystrophin-deficient diaphragm.[22] Overall, these studies show a remarkable increase in proteins identifiable from skeletal muscle tissue as LC–MS/MS instrumentation advances. Besides identifying proteins and validating them as function of genetic background or environmental factors, identifying signal transduction responsible for the observed changes is rare. Further, none of these studies quantified the proteome of cachectic patients or mimicked cachexia *in vitro* in order to understand the molecular pathology underlying cachexia disease, which leaves patients with a very poor prognosis.

Hence, we quantified the proteome of muscle biopsies from diagnosed cca patients and three control groups: weight-stable cancer (wsc), healthy non-sarcopenic (hns), and age-related sarcopenia (ars) using an advanced unbiased proteomics method termed SWATH-MS which takes advantage of the latest generation high mass accuracy mass spectrometers coupled to liquid chromatography (Schema 1A).[23] We found the muscle proteome composition in cca to be quantitatively different from control groups, identified protein modules representing this robust protein signature, and validated main components in a separate cohort of cca patients (Schema 1B). To further elucidate the molecular mechanisms of cachexia, we used myoblasts from an 83-year-old donor and quantified myogenesis as a function of time and perturbation using a single cytokine (tumor necrosis factor α, TNFα) (Schema 1C) to mimic the disease condition. Signal transduction changes as a function of perturbation were quantified using multiplexed antibody-based protein microarrays. Altered protein modules identified *in vitro* system were correlated back to patient derived proteomics data and confirmed by Western blotting.

Methods

Patients/volunteers

All participants gave written informed consent prior to study entry. All procedures were approved by the NHS Lothian Research Ethics Committee. The study conformed to the standards set by the Declaration of Helsinki.

DOI: 10.1002/jcsm.12188

Schema 1 Project overview. (A) There are four cohorts: cancer cachexia, weight-stable cancer, age-related sarcopenic, and non-sarcopenic. Latter two cohorts are defined as healthy elderly. Muscle needle biopsies were taken from patients and the proteome extracted using tissue grinding. Extracted proteins were digested and purified peptides analysed using liquid chromatography coupled to tandem mass spectrometer (LC–MS/MS). (B) Proteins were quantified across patients and statistical significance analysis performed. Third-order data integration was used to determine proteins of interest, especially differentiating between sarcopenic and cachexic patient groups. (C) Time-resolved myogenesis of myoblasts from an 83-year-old donor were grown for 72 h without perturbation and with single cytokine (tumor necrosis factor α (TNFα)). Immunohistochemistry data was supplemented with quantitative proteomics as a function of time using antibody-based protein arrays and LC–MS/MS.

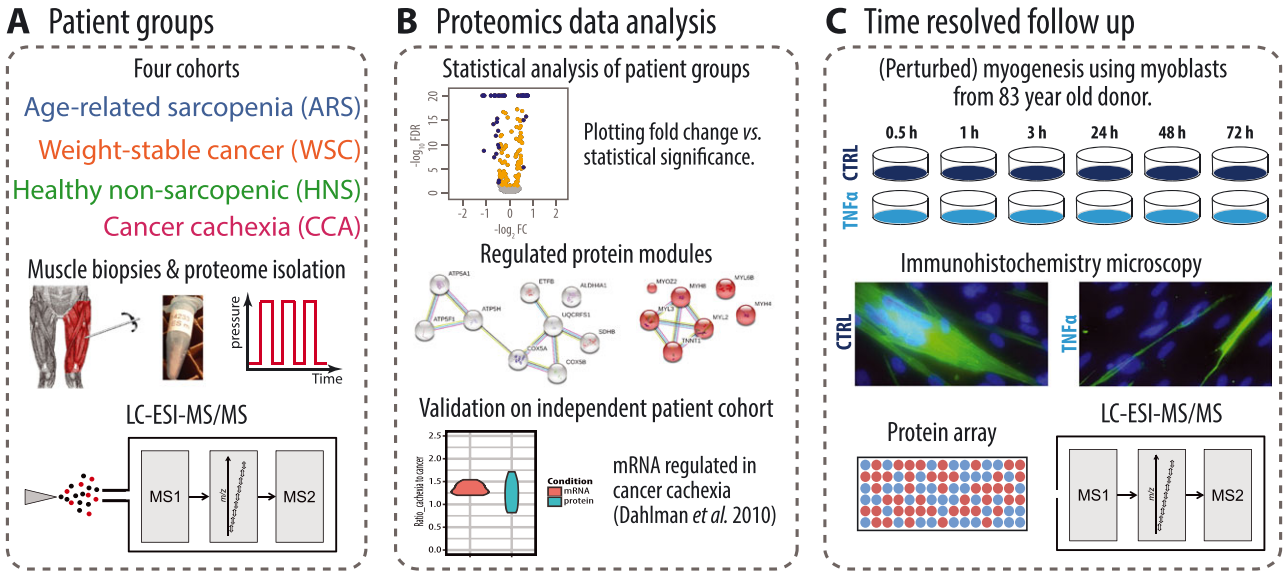

Nineteen cancer patients were identified via the upper gastrointestinal cancer multi-disciplinary team at the Royal Infirmary, Edinburgh, UK. Patients had newly diagnosed potentially resectable cancer. Pre-morbid weight was recalled by the cancer patients and verified where possible from the medical notes. Individual weight-loss was calculated and expressed as a percentage of pre-morbid body weight loss. Patients were considered cancer cachectic if they had lost more than 5% of their pre-morbid weight (23). The second group of cancer patients was considered as the wsc patients.

All healthy elderly participants aged >75 years were recruited using advertisements in local newspapers. Based on their responses to previously published health selection criteria,[7,24] all individuals were healthy and did not engage in any form of physical training. Based on DXA, these individuals were classified as non-sarcopenic healthy elderly or age-related sarcopenic. Criteria for this classification was based on the RSMI ((mass of skeletal muscle in kg) / ((body height in m)^2)) below 7.26 (men) and 5.45 (women).[25] C-reactive protein was measured in serum using an automated hospital-based technique (Abbott TDX).

A Bergstrom needle muscle biopsy was obtained from the lateral mass of the quadriceps under local anaesthetic. The biopsy was cleaned of gross blood contamination and snap frozen in liquid nitrogen and stored at −80 °C. Dual-energy X-ray absorptiometry (Hologic Discovery A) was used to measure body composition (i.e. fat mass, lean mass, and bone mineral content). See Table 1 for patient demographics.

Cell culture and treatment

Human skeletal muscle cells from an 83-year-old donor (HuSkMCs; Cook Myosite Inc, PA 15238, USA) were cultured for six days at 37 °C, 5% CO_2 in growth medium consisting of Myotonic basal medium (Cook Myosite Inc, PA 15238, USA) supplemented with Myotonic growth supplement (Cook Myosite Inc, PA 15238, USA), 20% FCS (Thermo Fischer Scientific), 100 μg/mL ampicillin (Sigma Aldrich), and 10 μg/mL Insulin (Amimed). Cells were then seeded in collagen-coated 96-well plates (25 000 cells/well) and in six-well plates (500 000 cells/well). After 24 h, cells were washed once with differentiation medium consisting of Myotonic differentiation medium (Cook Myosite Inc, PA 15238, USA) supplemented with 1% FCS (Thermo Fischer Scientific) and 100 μg/mL ampicillin (Sigma Aldrich). Cells were starved for 3 h at 37 °C in differentiation medium. Subsequently, HuSkMCs were treated with 1 ng/mL TNFα (R&D system) for different time frames (30 min, 1 h, 3 h, 24 h, 48 h, and 72 h). At the end of incubation, all the plates were washed with phosphate-buffered saline (PBS) and further processed for the different assays described below.

DOI: 10.1002/jcsm.12188

Table 1 Patient demographics

	Cancer patients (n = 19)		Healthy volunteers (n = 18)	
	Non-cachexia (n = 14)	Cachexia[a] (n = 5)	Non-sarcopenic (n = 10)	Sarcopenic[b] (n = 8)
M:F	12:2	3:2	6:4	4:4
Age	66.3 (10.2)	64 (4.1)	77.4 (2.3)	80.3 (3.9)
Weight (kg)	81 (14.7)	89.6 (19.1)	73.4 (13.8)	61.1 (7.7)
Height (cm)	174.6 (9.5)	170.2 (2.7)	165.1 (7.6)	163.5 (6.1)
BMI	25.9 (3.8)	25.8 (4.7)	26.6 (4.1)	22.8 (2.6)
% WL	2.3 (3.2)	15.9 (6.8)	—	—
LBM (kg)	47.2 (6.8)	43.7 (6)	50.3 (10)	43.3 (7)
FM (kg)	18.8 (6.4)	17 (3.5)	20.9 (6.4)	15.8 (4.2)
ASM (kg/m^2)	6 (0.6)	5.9 (0.8)	7.7 (1.3)	6.3 (0.9)
Cancer type		0	—	—
Gastric	1	1	—	—
Oesophageal	4	0	—	—
OGJ	2	4	—	—
Pancreas	7			
CRP (mg/L)	19.8 (44.7)	15.8 (17.3)	3.2 (2.5)	3.4 (2.8)
% > 10 mg/L	29	40	0	0

Values are mean and s.d.
[a]Defined by >10% WL.
[b]Baumgartner's criteria.

Immunofluorescence

Human skeletal muscle cells growing in 96-well plates were fixed with 4% paraformaldehyde and washed once with PBS. For permeabilization, cells were rinsed once in 0.5% Triton/cytoskeleton stabilizing buffer (80 mM PIPES, 5 mM EGTA, 1 mM $MgCl_2$, 40 g/L PEG3500 in distilled water) for 15 min. After washing with PBS, cells were incubated in 10% normal goat serum (Invitrogen) to avoid unspecific binding. Primary antibodies were diluted in PBS and incubated overnight at 4 °C. Cells were then washed twice with cytoskeleton stabilizing buffer and incubated with secondary antibody diluted in PBS for 1 h at room temperature. Images were acquired with CellR software (Olympus) on a fluorescence microscope (Olympus IX81-ZDC) and further processed with the Fiji program.

Protein extraction

Proteins were extracted from pulverized human skeletal muscle tissue by homogenizing the samples in the Precellys 24 system. Briefly, 300 μL of PhosphoSafe Extraction Reagent (Millipore) was added to minced and ground human skeletal muscle tissue (8 mg) in Precellys 24 lysing kit tubes. Tissue was further homogenized using the high-throughput homogenizer Precellys 24, for 10 s.). After incubation on ice for 5 min, the lysates were spun at 800 *g* for 5 min at 4 °C. Supernatants were transferred into new tubes and spun for another 12 min at 1600 *g* at 4 °C. Pellets (insoluble fraction) were stored at −80 °C until further us. Supernatants were collected and protein concentrations measured using the BCA Protein Assay Kit (Pierce) with BSA as a standard. Afterwards, phosphatase inhibitor cocktail (Roche) was added, and the samples were stored at −80 °C until further use. For protein extraction of human muscle cells, the same method was used. Human skeletal muscle cells cultured in six-well plates were lysed with 200 μL of PhosphoSafe Extraction Reagent (Millipore) following the same procedure using the Precellys 24 system for homogenization.

Western blot

Ten micrograms of protein extracts in reducing Laemmli SDS sample buffer was boiled for 5 min at 95 °C and then separated by sodium dodecyl sulfate polyacrylamide gel electrophoresis on 4–20% gradient gels (Bio-Rad, Cressier, Switzerland), blotted to nitrocellulose membranes (Bio-Rad) using the Trans-Blot Turbo Transfer System (Bio-Rad), blocked for 1 h in blocking buffer (5% non-fat milk in Tris-buffered saline 0.05% Tween-20), incubated overnight with primary antibody, rinsed, and incubated for 1 h with peroxidase-conjugated goat anti-rabbit IgG at room temperature. Blots were developed using enhanced chemiluminescence (Roche, Rotkreuz, Switzerland) or SuperSignal West Femto substrate (Thermo Scientific, Wohlen, Switzerland) and exposed to Kodak film (Kodak, Rochester, NY, USA). Antibodies used were ERK1/2 mouse monoclonal clone L34F12, P-ERK1/2 (Thr202/Tyr204) (197G2), and Tubulin (11H10) were from Cell Signaling Technologies (Danvers, MA, USA). ATP5A (7H10BD4F9) to ATP5H (7F9BG1) were from Abcam (Cambridge, UK); ROCK1 Antibody (EP786Y) from Novus Biologics (Littelton, CO, USA), Anti-β-Actin, Clone AC-74 from SIGMA (St Louis, MO, USA); Rabbit polyclonal: Phospho-FAK (Tyr576/577), Phospho-FAK (Tyr397), and FAK were from Cell Signaling Technologies (Danvers, MA, USA); Troponin I fast skeletal and mtHSP70 were from Abcam (Cambridge, UK); rabbit monoclonal Phospho-NF-kB p65 (93H1) (Ser536), Cofilin (D3F9), Phospho-Akt (Thr308) (244F9), Phospho-Cofilin (Ser3)

DOI: 10.1002/jcsm.12188

(77G2), and Akt (pan) (11E7) were from Cell Signaling Technologies (Danvers, MA, USA)

Western blots were analysed densitometrically using ImageJ software version 1.45 (NIH, Bethesda, MD, USA; http://rsbweb.nih.gov/ij). Band intensity of each sample was normalized to coomassie blue stained gels.

Immunohistochemistry

The following antibodies were used: immunofluorescence primary antibodies: mouse α-Myosin (skeletal, fast) (1:500, Sigma), rabbit α-Desmin (1:200, Sigma), secondary antibodies: goat α-rabbit IgG (H + L) alexa fluor 488 F (ab′) 2 fragment (1:750, Invitrogen), and goat α-mouse IgG (H + L) alexa fluor 488 F (ab′) 2 fragment (1:750, Invitrogen).

Protein array

The Kinexus Antibody Microarray KAM-850 analyses were performed on protein lysates of HuSkMCs. Cells were lysed in 200 μL per well using KAM-850 kit lysis buffer. Protein lysates were transferred in mpbio lysing matrix D tubes, and preparation was conducted using a fast prep machine (MP Biomedicals) as described in the protocol and on the Kinexus Internet Web site at www.kinexus.ca. Briefly, 50 μg of HuSkMc lysate proteins was labeled with the kit fluorescent dye at a concentration of 2 mg/mL, and unincorporated dye molecules were removed by centrifugation on desalting columns (provided in the kit), and total fluorescence was measured on a Spectramax Paradigm® reader using the Tune Cassette (Molecular Devices, Sunnyvale, CA). Purified labeled proteins from two samples were incubated separately on opposite sides of a KAM-850 antibody microarray. This microarray features two identical fields of antibody grids, each field containing 517 pan-specific antibodies and 337 phospho-site-specific antibodies. These antibodies are printed in duplicate. After probing, arrays were scanned using a GenePix® scanner (Molecular Devices, Sunnyvale, CA) with a resolution of 10 μm, and resulting images were quantified using GenePix® Pro 7 software (Molecular Devices, Sunnyvale, CA). Values provided in the figures are the means of the recorded measurements from each antibody spot pair normalized with the total Protein Fluorescence obtained and measured after labeling.

Cell lysis and peptide generation for liquid chromatography coupled to tandem mass spectrometer analysis

A detailed protocol for lysis and peptide clean-up for LC–MS/MS can be found in the Supporting Information peptide cleanup.

Liquid chromatography coupled to tandem mass spectrometer analysis

The LC–MS/MS system used was an Eksigent NanoLC Ultra 2D Plus HPLC system coupled to a 5600 TripleTOF mass spectrometer (Sciex, Framingham, MA). Samples were chromatographed using a 1D 2-h gradient from 2 to 35% (buffer A 0.1% (*v/v*) formic acid, 2% (*v/v*) acetonitrile, buffer B 0.1% (*v/v*) formic acid, 90% (*v/v*) acetonitrile) after direct injection onto a 20-cm PicoFrit emitter (New Objective) packed to 20 cm with Magic C18 AQ 3-μm 200-Å stationary phase. For MS/MS acquisition in shotgun mode, top 20 most intense MS1 precursors (collected between 360 and 1460 *m/z* for 250 ms) with charge states between 2 and 5 selected for MS2 fragmentation, with a 15-s exclusion window. Fragment MS2 ions were collected for 100 ms across a 50–2000 *m/z* range. For MS/MS acquisition in SWATH-MS mode,[23] fragment windows were chosen as listed in the Supporting Information (SWATH data analysis) and identical LC gradient listed above. For anchoring SWATH maps during the subsequent targeted analysis, reference iRT peptides (Biognosys, Schlieren, Switzerland) were spiked into the sample with a dilution of 1:20 *v/v*.

Shotgun data analysis

For targeted extraction of ion chromatograms from SWATH-MS maps, four cell line samples (untreated and TNFα at 0.5 h and 72 h) were analysed in shotgun mode. The spectra were searched using the search engines X!TANDEM Jackhammer TPP (2013.06.15.1—LabKey, Insilicos, ISB) and Comet version '2013.02 rev. 2' against the uniprot canonical human protein (reviewed) database using Trypsin digestion and allowing one missed cleavage. Included were 'Carbamidomethyl (C)' as static and 'Oxidation (M)' as variable modifications. The mass tolerances were set to 15 ppm for precursor ions and 0.1 Da for fragment ions. The identified peptides were processed and analysed through the Trans-Proteomic Pipeline (TPP v4.7 POLAR VORTEX rev 0, Build 201403121010) using PeptideProphet, iProphet, and ProteinProphet scoring. Spectral counts and peptides for ProteinProphet were filtered at false discovery rate (FDR) of 0.01 iprophet-pepFDR (=0.759 iprob). This analysis resulted in 1751 proteins at 1% FDR (E1501221230) identified with at least one peptide per protein.

SWATH data analysis

Sequential acquisition of all theoretical masses (SWATH-MS) allows for consistent quantification of proteins between patient groups. SWATH-MS uses a time of flight mass analyser in combination with a fast high mass accuracy mass

DOI: 10.1002/jcsm.12188

spectrometer enabling consistent quantification of peptides across many samples. Hence, if a peptide is not detected in SWATH-MS mode, it fell below the limit of detection, and the stochastic sampling approach of traditional shotgun experiments does not apply. For targeted extraction, a custom SWATH-library was built using standard parameters,[26] and all SWATH assays deposited into a publically available SWATH library.[27] SWATH-MS maps were analysed using OpenSWATH workflow[28] (Supporting Information SWATH analysis). Protein abundance values were calculated with two peptides per protein minimum using aLFQ[29] for *in vitro* myogenesis experiments, while mapDIA v2.2.0[30] was used for statistical analysis of patient data.

Results

Proteome isolation of muscle biopsies

To characterize cca in muscle tissue on a proteomics level, we collected human biopsies (*N* = 36, Table 1). The samples included healthy non-sarcopenic healthy elderly (hns, *N* = 10), weight-stable cancer (wsc, *N* = 14), age-related sarcopenia (ars, *N* = 8), and cachectic cancer patients (cca, *N* = 4). The extracted soluble proteome was analysed using high mass accuracy mass spectrometers operated in SWATH-MS mode, which is a non-stochastic protein quantification method allowing for consistent quantification of analytes between patient-derived samples.[23] The resulting digital record was analysed *in silico* (see for details, *Figure* 1A). Initial protein analysis per patient revealed that some patient proteome profiles either contained a very low amount of protein IDs or predominantly contained albumin and haemoglobin dominating protein abundance measurements, suggesting a high blood component within the muscle biopsy. Those samples were excluded resulting in 26 muscle biopsies that were used for further analysis. Normalized values for 521 proteins across 26 samples are shown in an unsupervised clustered heat map using Pearson correlation distance function (*Figure* 1B). Next, we calculated the median coefficient of variance (CV) per patient group to be 0.4 (*Figure* 1C), which is good considering a technical CV of 0.2 and quantification of primary patient material.

Alteration of muscle composition in cachexia

We first compared proteome signatures from both healthy elderly groups with wsc patients using mapDIA (see Supplementary Data 1-mapDIA). This comparison resulted in 25 proteins with a statistically significant score of FDR $< 9{\cdot}10^{-19}$, while only seven proteins were at least two-fold differentially regulated between patient groups (*Figure* 1D, upper panel). The only muscle protein group with a differential protein expression was muscle contractile myosins (myosin heavy chain 1, 2, 3, 6, 7, 8: 7-MYHs) in which expression in healthy elderly was reduced compared with wsc patients (FC $\log_2 = -1.5$, FDR = $6.7{\cdot}10^{-10}$). Next, we compared proteomes from cca with wsc patients. Statistical significance analysis resulted in 57 proteins with a FDR $< 9{\cdot}10^{-19}$ of which 44 proteins were at least two-fold differentially expressed between the patient groups (*Figure* 1D, lower panel). Lower expressed in cachectic vs. wsc patients were Tropomyosin TPM1, 2 (FC $\log_2 = -1.7$, FDR $< 9{\cdot}10^{-19}$) together with a higher expression of muscle contraction myosins (myosin heavy chain 1, 4, 8: 3-MYHs) (FC $\log_2 = 2.3$, FDR $< 9{\cdot}10^{-19}$), suggesting a dramatic change in conventional muscle composition in cachectic muscles vs. muscles of wsc patients. Similarly, the comparison of cachectic vs. healthy elderly muscle biopsies (*Figure* 1E, left panel) showed higher expression of muscle contraction myosins (myosin heavy chain 1, 2, 4, 8) in cca samples (FC $\log_2 = 1.6$, FDR $< 9{\cdot}10^{-19}$). Third, we compared ars with cca and identified 34 proteins with a statistically significant score of FDR $< 9{\cdot}10^{-19}$, while 29 proteins were at least two-fold differentially expressed between the groups (*Figure* 1E, right panel). Among the highest differentially regulated proteins were muscle contraction myosins (myosin heavy chain 1, 4, 8) with a FC $\log_2 = 2.3$ (FDR $< 9{\cdot}10^{-19}$) which were more highly expressed in cachexia compared with age-related sarcopenic muscle. From these three analyses based on statistical significance and fold change, or ratio between conditions (FC) we conclude that cca has a distinguishable proteome compared with two other groups: healthy elderly (both sarcopenic and non-sarcopenic) and wsc patients. There was no comparable proteome signature identified in any other comparison between groups (see Supplementary Data 1-mapDIA). Even within the healthy elderly group separated based on the RSMI into non-sarcopenic and sarcopenic individuals, little change in the actual proteome was observed. Hence, our proteome analysis of needle biopsies of various cohorts revealed that cca may be associated with specific protein markers.

Differentiation of cachexia vs. all other patient groups

Our proteome analysis based on LC–MS/MS demonstrated that there are two main groups: cachexia vs. all other elderly (healthy sarcopenic and non-sarcopenic), and wsc. Although the limited sample size does not allow for any sophisticated statistical analysis, we wondered if there were any functional modules differentially regulated between the patient groups. To address this question, we median centred protein values for the cachexia and all other patient samples. If the ratio of these two median protein values was less than 0.5 or more than 2, we considered them regulated. There were 89

Figure 1 Proteomics data. (A) Overview of computational analysis of liquid chromatography coupled to tandem mass spectrometer (LC–MS/MS) data acquired in SWATH mode. First, the mass spectrometer acquires the *m/z* ratio in a data independent fashion. Areas under the curve of co-eluting transitions are the basis for peptide quantification. Automatically annotated peptides are filtered based on quality scores and give rise to protein quantification, which are further analysed by mathematical and statistical algorithms. (B) Heatmap of all proteins quantified per patient (ars: age-related sarcopenia, cca: cancer cachexia, hns: healthy non-sarcopenic, wsc: weight-stable cancer). (C) Violin plots of coefficient of variance (CV) per patient groups. (D, E) Volcano plots of statistical significance analysis focusing on cachexic vs. other patient groups.

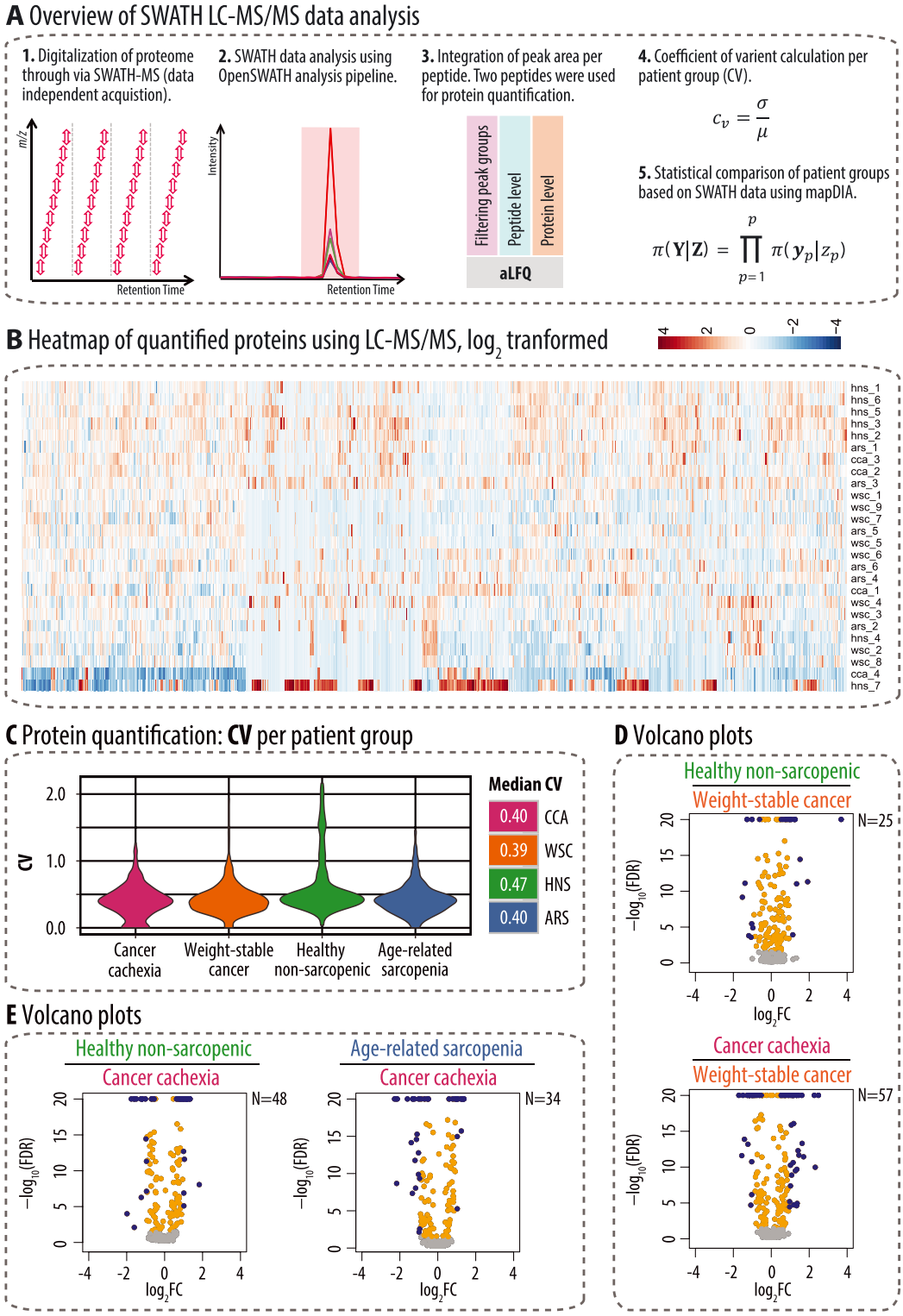

DOI: 10.1002/jcsm.12188

regulated proteins which were then analysed by STRINGv10[31] for high confidence (>0.9) interactions with experimental evidence. The STRINGv10 analysis clustered into four functional entities: heme cluster, Fo complex, electron transfer chain, and contractile fibre (see Supplementary Data-89_prot_sig). We excluded the heme cluster from further analysis as this is most likely a result of muscle biopsy procedure variance and not disease related. Focusing on the remaining functional modules (*Figure* 2A), we chose 16 representative proteins and plotted Euclidean distance clustered protein values in a heat map shown in *Figure* 2B. Using this 16 protein signature, cachectic patients are grouped in a cluster, and as little as two components could explain 90% of the variance (*Figure* 2C). Intriguingly, using this 16 protein signature, a healthy individual clustered with cca patients, which we speculate could indicate an undetected underlying chronic disease causing cachexia in this individual. We are currently collecting additional muscle biopsies to identify which of these 16 proteins are resulting in a statistically significant protein signature able to differentiate between cachectic and wsc patients.

To further support and validate protein modules identified in our proteomics study, we compared our proteomics results based on LC–MS/MS to global gene expression profiles based on mRNA microarray data from gastrointenstinal cancer patients (N = 14) with cca (N = 13).[32] Overall, our proteomics data show a larger dynamic range of regulated proteins comparing cca to weight stable cachexia patients (*Figure* 2D). Our work and data from Dahlman and coworkers clearly show a dysregulation of proteins GO annotated as mitochondrial electron transport chain and focal adhesion (*Figure* 2D). As both studies identified identical pathways dysregulated in cca using alternative protein quantification methodologies and independent patient cohorts, we believe that further proteome quantification of cca muscle biopsies will undoubtedly result in a robust protein signature consisting of two or three proteins.

Time-resolved in vitro follow-up

Based on muscle biopsy proteomes, our initial pilot study identified only two patient groups. Hence, we asked which molecular mechanisms could underlie the observed changes. To address this question, we turned to an *in vitro* myogenesis system using human primary myoblast of an 83-year-old donor which was commercial available from COOK Myosite. Myoblasts were seeded and grown under standard cell culture conditions. To mimic perturbation typical of cachexia, we added TNFα. In a time lapse experiment, we characterized (perturbed) myogenesis using immunohistochemistry, antibody-based protein array for quantifying signal transduction changes and undepleted proteome quantification using LC–MS/MS in SWATH-MS acquisition mode (Schema 1C).

To characterize the morphological changes of our *in vitro* system, we stained cells with antibodies against different filament systems (myosin heavy chain 2 and desmin) and with nuclear stain 4",6-diamidino-2-phenylindole (DAPI). The resulting immuno-histochemistry was visualized by fluorescence microscopy. Representative pictures showing the progress of myogenesis are shown in *Figure* 3. *Figure* 3A, top row, shows myogenesis as a function of time under normal conditions using a myosin-fast antibody, which is a marker for terminal differentiation. A characteristic progression of single cell (myoblast) to myofibres within 48 h is observed, which is in contrast to TNFα-treated myoblasts where no significant myofibre formation is seen (*Figure* 3A, bottom row). TNFα-treated cells appear to be trapped at a precursor state, which morphologically resembles untreated cells at 24 h. *Figure* 3B depicts a zoom-in of myofibre structures of untreated (*Figure* 3B, left panel) multi-nucleated myofibres. In contrast, TNFα-treated myoblasts form only single myosin strands (*Figure* 3B, right panel). *Figure* 3C shows comparable staining of untreated and treated cells with Desmin (green) and nuclei with DAPI (blue). From our results, we conclude that failed myofibre formation under TNFα treatment is not due to loss of viability. However, proteome quantification using SWATH-MS methodology of the same time samples shows a clear shift in proteins identified comparing early with late time points. This shift in the proteome was also found in the cytokine-treated cells indicating ongoing differentiation of the cells (*Figure* 3D).

Signal transduction characterization

To explore what might cause the observed phenotypic impairment, we quantified 332 epitopes using antibody-based protein microarray (Kinexus) of untreated and TNFα-treated myoblasts from an 83-year-old donor at 0.5, 1, 3, 24, 48, and 72 h. First, we plotted the ratio of TNFα/untreated epitopes per time point as violin plots (*Figure* 4A); hence, the closer the values are to 1, the more similar are the two conditions to each other. Overall, there appear to be two responses: an initial response at 0.5 h, which diminishes at 1 h with most epitopes of equal intensity in both TNFα-treated and untreated samples. Starting at 3 h, a constant increase in ratios can be observed until the maximum at 48 h; 48 h exhibits also the largest difference in morphology between the two treatment conditions: in untreated cells, myofibres appear, while in TNFα-treated cells, only sporadic myofibre precursors are apparent (*Figure* 3A**)**. Finally, at 72 h, the differences in epitopes quantified by protein microarrays slowly diminish (*Figure* 4A). From this global analysis, we conclude that even relatively small and transient changes in phosphorylation levels caused by treatment with TNFα are sufficient to cause incomplete myogenesis in treated cells.

Figure 2 Third-order data analysis. (A) Protein–protein interaction analysis of highly regulated proteins with statistical significance resulted in three modules distinguishing cachexia from all other patients or healthy elderly. (B) Heatmap of proteins representing protein clusters identified above (ars: age-related sarcopenia, cca: cancer cachexia, hns: healthy non-sarcopenic, wsc: weight-stable cancer). (C) Principle component analysis of protein signature demonstrating that three proteins would be able to explain the variance differentiating between cachexic and all other patient groups. (D) Cross validation of identified protein modules by alternative protein abundance measurements on independent cohort.[32]

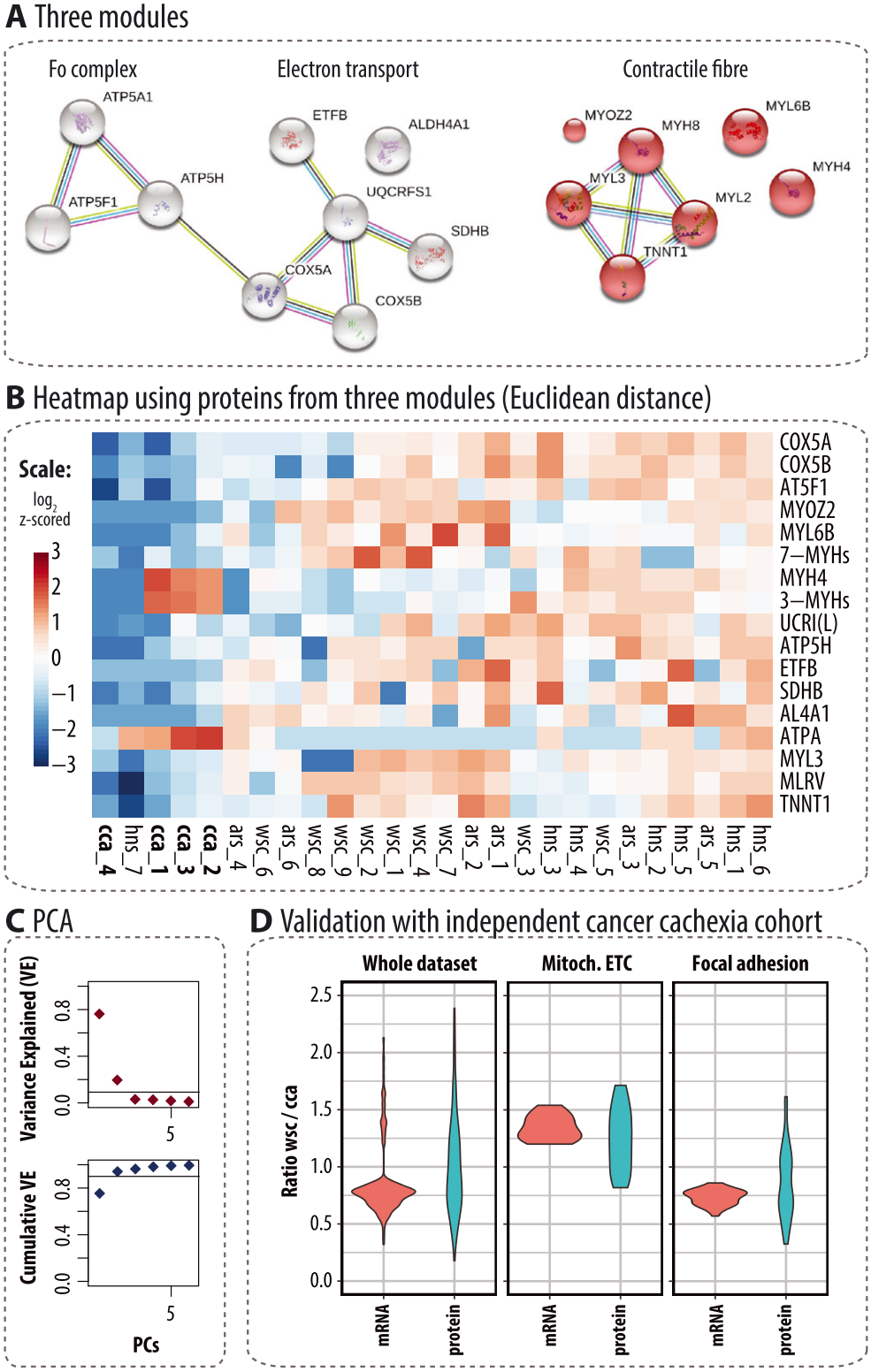

DOI: 10.1002/jcsm.12188

Figure 3 Immunohistochemistry of myogenesis. (A) Myogenesis as a function of time (3 to 72 h) and perturbation using tumor necrosis factor α (TNFα). In blue, cell nuclei are stained using 4″,6-diamidino-2-phenylindole (DAPI), while in green, myosin-fast antibodies were used to stain for myofibres. (B) Zoom-in of terminal time point at 72 h: clearly visible are the multi-nucleated myofibres in the untreated cells. In contrast, TNFα-treated myoblasts did not differentiate into myofibres. (C) Use of Desmin antibodies and DAPI staining demonstrates that muscle cells are viable in both conditions. (D) Proteome quantification using SWATH-MS: a four-way Venn diagram shows the proteome shift as a function of time and perturbation. The heatmap shows protein values of differentially regulated proteins as sorted by Pearson correlation.

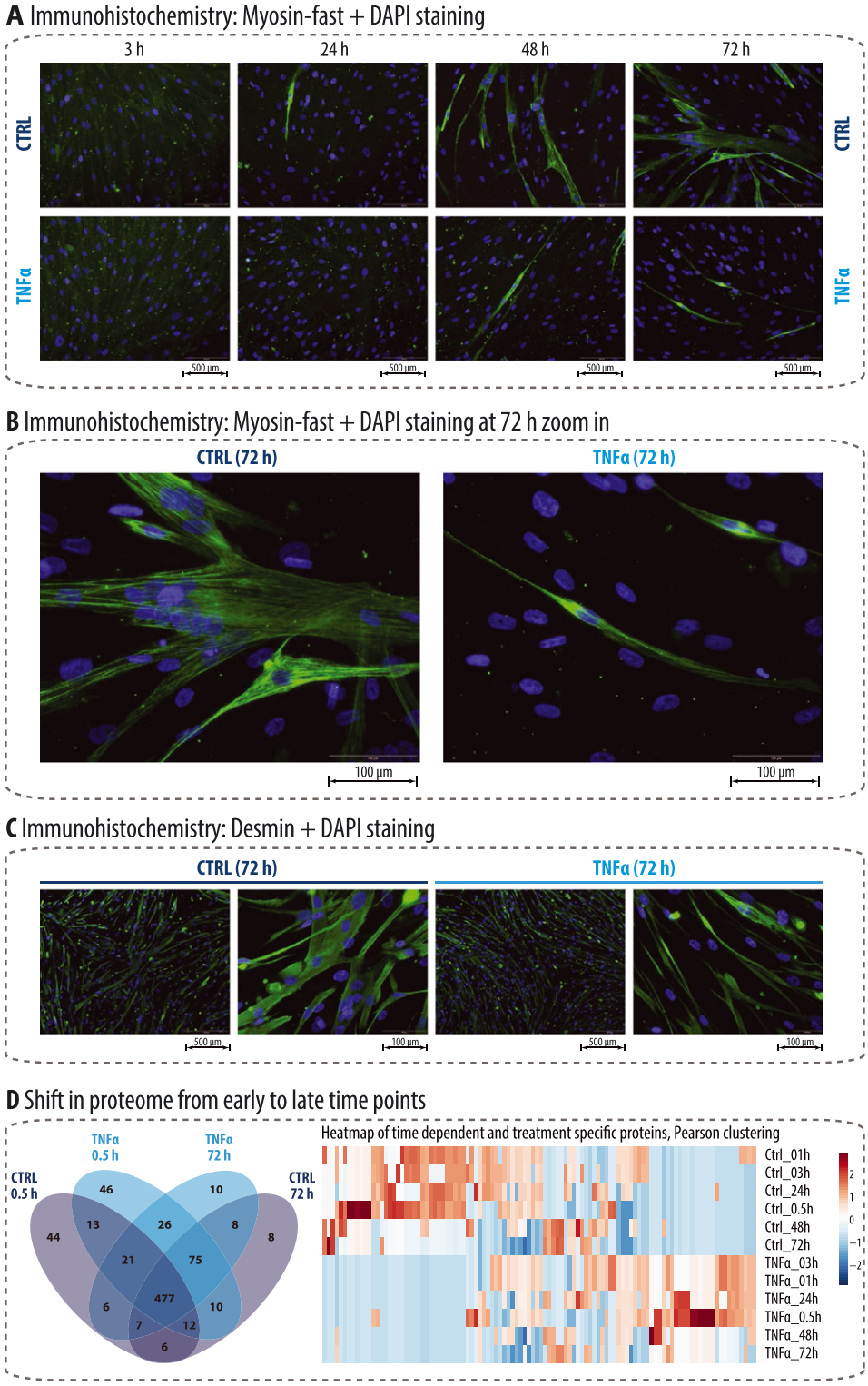

DOI: 10.1002/jcsm.12188

Figure 4 Time-resolved orthogonal proteome analysis. (A) Violin plot depicting ratio of TNFα/untreated from 332 protein epitopes quantified by protein array as function of time. (B) Individual key proteins selected from protein array data and normalized epitope values plotted as function of time. Untreated values are shown in dark blue, while TNFα-treated cells are shown in light blue.

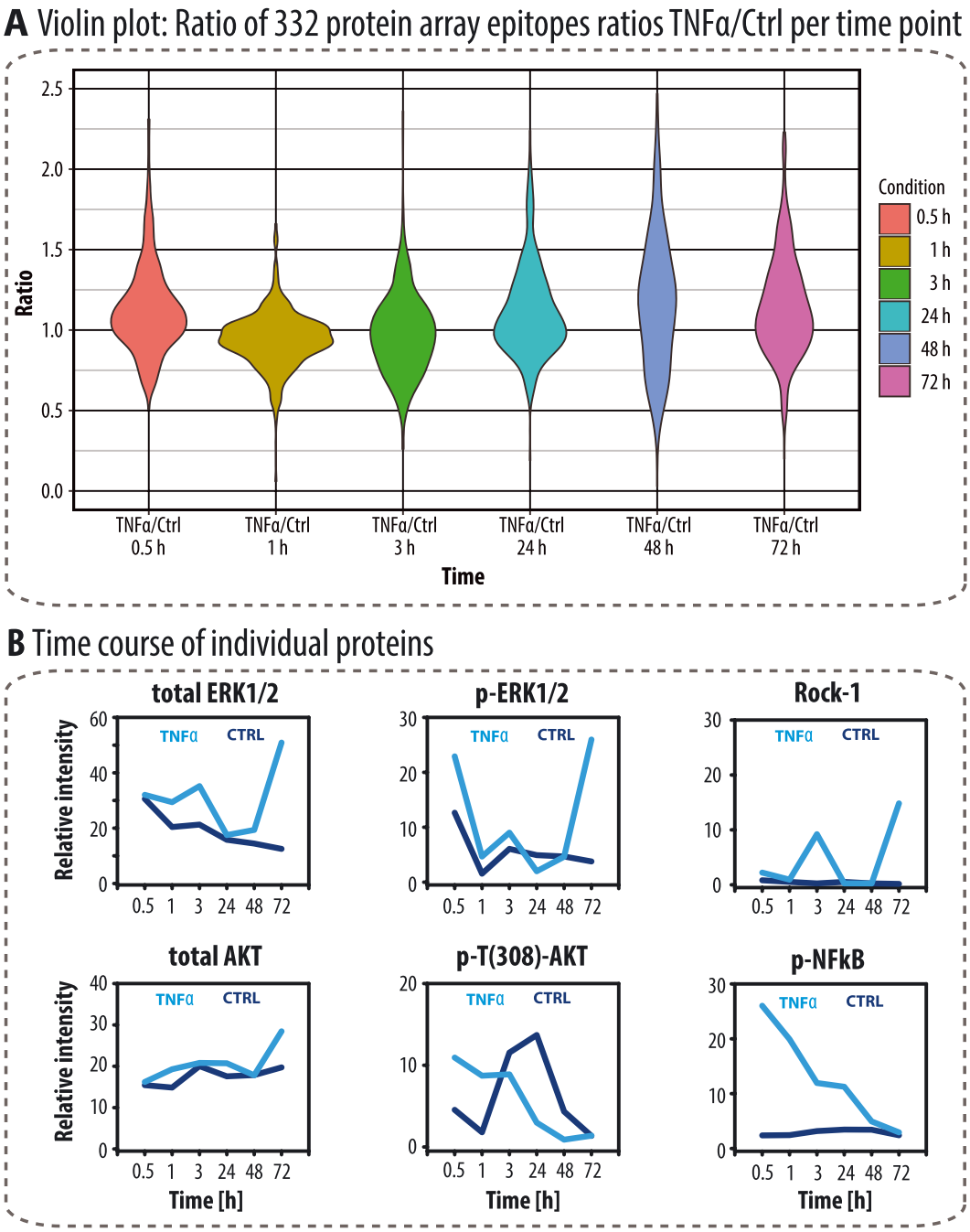

Next, we interrogated individual quantified epitopes. One example of expected differential protein signaling is phosphorylated Nuclear factor NF-kappa-B. Nuclear factor NF-kappa-B (NFkB) should remain non-phosphorylated in untreated cells, while upon cytokine treatment, the transcription regulator NFkB will be activated through phosphorylation. As seen in *Figure* 4B, our antibody-based protein array data confirmed by Western blotting support exactly the predicted pattern of high levels of p-NFkB in TNFα-treated cells during early time points, while only background levels of p-NFkB were observed in untreated cells. Interestingly, levels of phosphorylation in treated cells

DOI: 10.1002/jcsm.12188

are restored to background levels only after 72 h. To confirm inflammatory pathway activation, we determined phosphorylation levels of P38. We detected a five-fold increase in p-P38 levels at 0.5 h comparing untreated to TNFα-treated myoblasts. Throughout the time course, p-P38 levels in TNFα-treated cells were generally higher than in untreated cells (see Supplementary-p-P38.pdf) Alongside the detection of p-NFkB upon TNFα treatment, additional phosphorylation of proteins was detected exclusively under this condition. ERK1/2 is one such example in which total ERK1/2 increases as a function of time and TNFα treatment, while in untreated samples total ERK1/2 steadily decreases. Phospho-ERK1/2 (p-ERK1/2) decreases as a function of time in both TNFα-treated and untreated samples, while at 72 h p-ERK1/2 is five times higher in TNFα-treated cells (*Figure* 4B). Similarly, ROCK1 has a low expression level in untreated cells, while at 3 and 72 h the protein is expressed at high levels in TNFα-treated samples (*Figure* 4B). Another typical behaviour is a time-dependent activation and deactivation as a function of time in untreated cells, e.g. p-Thr (308)-AKT (*Figure* 4B). Although total AKT remains similar throughout the time course in both untreated and treated samples, there is a clear constant decrease of p-Thr (308)-AKT signal in TNFα-treated cells, while in untreated cells there is an activation of this phosphorylation site starting after 1 h and ending at 72 h. The p-Thr (308)-AKT signal co-insides with the morphological appearance of myofibres in untreated cells (see *Figure* 3A). It is intriguing to note that p-Thr (308)-AKT level at the final 72 h time point is equal between the two conditions. Another example of zero end point difference is the aforementioned p-NFkB (*Figure* 4B). These examples illustrate the importance of quantifying phosphorylation and protein abundance changes throughout myogenesis as single end-point analysis would have missed key regulatory differences, e.g. p-NFkB.

Cell fusion

Focal adhesion kinase (FAK) plays a pivotal role in modulating fusion of cells. Protein levels of FAK remain constant throughout myogenesis (*Figure* 5A) in untreated and TNFα-treated cells. However, autocatalytic phosphorylation at Tyr397 is down-regulated two-fold in TNFα compared with untreated cells at the 3 and 72-h time points (*Figure* 5A). At the same time points, phosphorylation of RET and SCR at Thr 576/577 is down-regulated four- and six-fold, respectively, in TNFα-treated cells. Furthermore, under TNFα treatment, levels of Thr 567/577 are four times higher at 30 min. Taken together, proper myogenesis and formation of multi-nucleated myotubes occur only in untreated cells, where FAK phosphorylation levels of Thr 567/577 slowly increase in early time points and stay constant throughout the time course. We see a correlation of impaired myogenesis when FAK Thr 567/577 phosphorylation levels fluctuate by as much as 10-fold throughout the time course in TNFα-treated cells. A time-lapse animation (Supplementary Data-hsadd04510_frames.gif) shows how different parts of the FAK signaling pathway are differentially activated as a function of time and perturbation.

In untreated myogenesis, cofilin, a protein implicated in cytoskeleton dynamics, steadily increases protein and phosphorylation levels until it doubled in intensity comparing 30-min with 72-h time points (*Figure* 5B). This is in contrast to TNFα-treated cells where total cofilin is twice as high at 3 h and phosphorylation levels nearly five times higher in TNFα compared with untreated at the same time. Further, total and phosphorylated levels of cofilin spike again at 72 h compared with untreated cells (see *Figure* 5B). This bimodal behaviour of increased protein amounts is mirrored in tubulin (*Figure* 5B) and pan-actin (*Figure* 5A), but not F-actin which remains nearly unchanged throughout myogenesis (*Figure* 5A). It appears as if the amount of pan-actin is less important in myogenesis than the steady 10-fold increase of troponin (fast) per time point (comparing 24 h to 48 h and 48 h to 72 h) as shown in *Figure* 5C. The drastic troponin (fast) increase coincides with appearance of myotubes (see *Figure* 3A).

Our data suggest that TNFα blocks myotube formation via dysregulation of key molecules of the FAK signaling pathway resulting in dysregulation of proteins involved in cytoskeleton dynamic and blocking of cell fusion.

Mitochondrial energy metabolism

Besides structural proteins, we also noted a dysregulation of proteins involved in the mitochondrial electron transport chain upon TNFα treatment. Under normal conditions, members of the mitochondrial ATP synthase complex (F_1 F_0 ATP synthase or Complex V) are more abundant at the 48 and 72-h time points when compared with earlier time points (see *Figure* 5C). In case of ATP5L and ATPO, both proteins are not detectable at early time points, while they are detectable at 48 and 72 h. ATPB is twice as abundant at 48 and 72 h when compared with earlier time points. Upon TNFα treatment, ATP synthase complex protein members are less well coordinated. ATPO is detected only at the 48 and 72-h time points, while ATP5L is already detectable in early time points. ATPB, which doubles in abundance in untreated cells, remains constant under TNFα treatment. We conclude that myotube formation in untreated myoblasts requires higher energy consumption, which is reflected in the increased amount of mitochondrial ATP synthase complex.

DOI: 10.1002/jcsm.12188

Figure 5 Time-resolved orthogonal proteome analysis of individual proteins and phosphorylation sites thereof: (A) focal adhesion pathway, (B) thin muscle filament, and (C) energy homeostasis with dark blue lines representing untreated and light blue TNFα-treated cells.

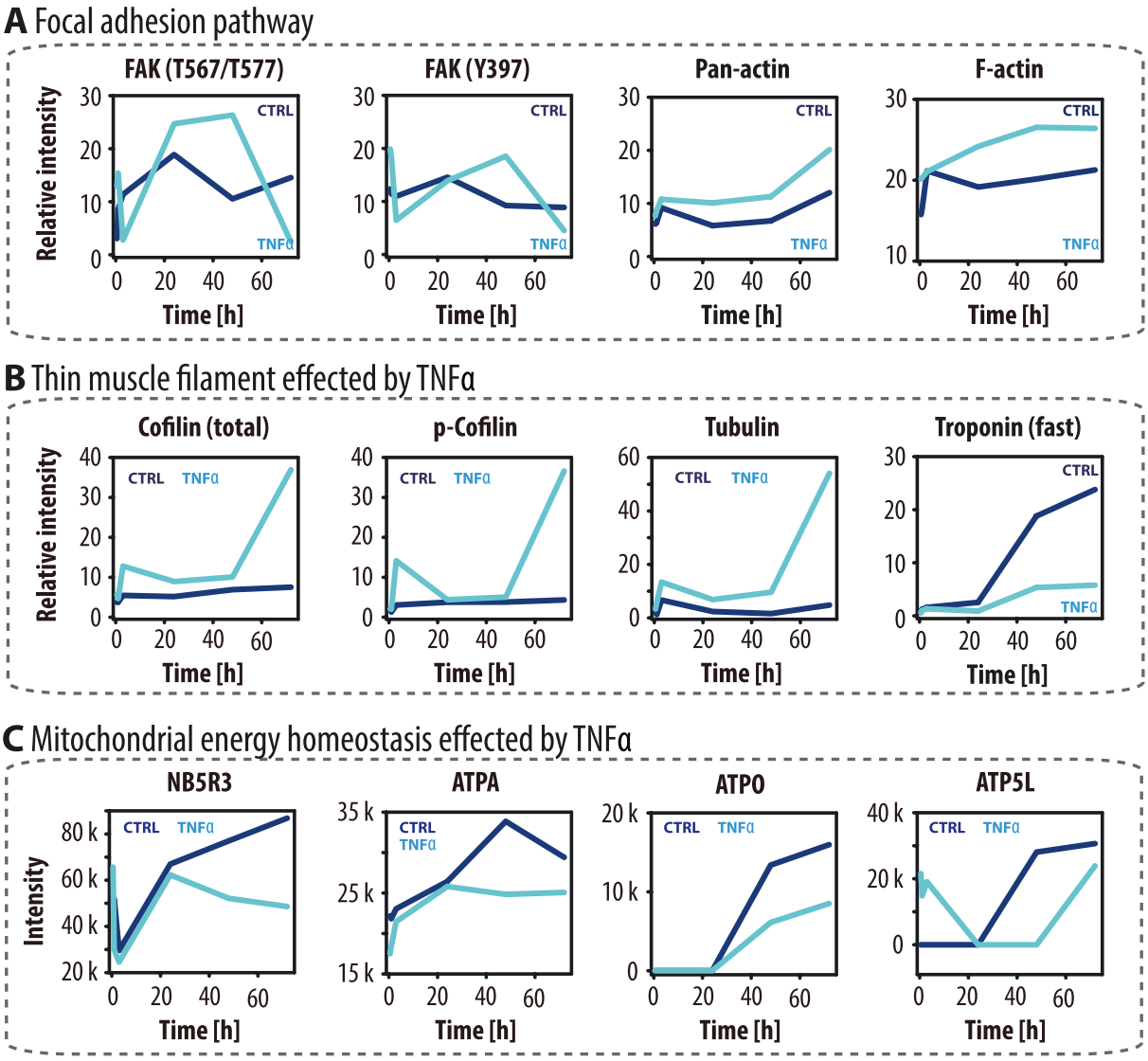

Discussion

Time lapse (perturbed) myogenesis proteome quantification

In an *in vitro* experiment, myoblasts from an 83-year-old donor differentiated into myofibre. Our time lapse quantification throughout myogenesis was essential to uncover dynamics otherwise missed by endpoint comparisons, e.g. single endpoint comparison between untreated and TNFα-treated cells at 72 h would have missed the dynamics of pNFkB entirely (*Figure* 4B). Other notable differences were the detection and quantification of matrix metalloprotease-14 (MMP-14) exclusively at the early time points of unperturbed myoblasts but not in TNFα-treated cultures. Matrix metalloprotease-14 is vital for the migration of myoblasts into collagen I matrix[33] and was also detected in the secretome of myoblasts during differentiation.[34] Hence, our data suggest that TNFα interferes at a very early stage of myogenesis with expression of proteins involved in muscle regeneration.

Our orthogonal investigation of myogenesis using immunohistochemistry, protein arrays quantifying phosphorylated epitopes and protein abundance measurements using SWATH-MS clearly shows that an orchestrated sequence of signaling events together with protein abundance changes results in myogenesis. Through the time course, observed phosphoproteme changes were small and transient upon TNFα treatment. Our data suggest that TNFα blocks cell fusion via the FAK signaling cascade (*Figure* 5). As a consequence of FAK

DOI: 10.1002/jcsm.12188

signal transduction perturbation, cellular actin structures are formed but do not result in fused cells as evidenced by immunohistochemistry. One possible mechanism of blocked actin filament formation could be due to phosphorylation of cofilin.[35] Our data support this possible mechanism as there is twice as much unphosphorylated cofilin in untreated myoblasts at 72 h than in TNFα-treated cells (*Figure* 5).

Identification of cachexia-specific protein signature supported by in vitro time course data

We set out to characterize proteome changes based on LC–MS/MS in skeletal muscles of cca patients and compared this group to three related cohorts: hns, ars, and wsc. Through consistent protein quantification by acquiring LC–MS/MS data in SWATH mode and fold change analysis, we identified the cachexia proteome to be distinct from all other cohorts in our study. The fold change analysis was followed by a protein network analysis which revealed three distinct functional modules affected by cachexia: Fo complex, electron transport chain, and contractile fibre. Reduced levels of electron transport chain proteins were also reported for skeletal muscles of chronic obstructive pulmonary disease patients.[36] Dysregulation of mitochondrial electron transport chain and focal adhesion was also observed by Dahlman and co-workers in cca patients.[32] Our results show that the combination of mitochondrial dysfunction and contractile fibre alterations will hold the key to a cachexia-specific protein signature.

This protein signature originating from patient muscle biopsies is further supported by our *in vitro* myogenesis experiments in which myoblasts differentiate into myofibres or arrested in pre-myofibre state due to treatment with TNFα. Quantifying the proteome as a function of time, we found that the ATP synthase complex is up-regulated at the later time points of myogenesis, suggesting that myotubes have an elevated energy consumption in comparison with single cell myoblasts as quantified by both LC–MS/MS and antibody-based protein arrays. In patient samples quantified by SWATH-MS, ATP synthase complex was identified in the initial 89 protein signature based on fold change and statistical significance analysis. The complex also propagated to the final protein signature as multiple complex members showed large fold changes and proteins were connected by high confidence protein–protein interactions (STIRNGv10). ATP5A was orthogonally quantified using Western blotting and is a promising candidate for a final protein signature able to reliably identify cachectic patients. We are collecting additional skeletal muscle samples from cachectic and weight-stable patient groups and will quantify the identified protein signature across a larger cohort of patients using targeted proteomics[37] to identify a robust protein signature of cachexia with statistical significance.

Protein signature for altered skeletal muscle regeneration

Our study focused on altered muscle regeneration as a consequence of cancer, an underlying chronic disease. It should be noted that not all cancers necessarily cause cachexia.[38] Similarly, skeletal muscle regeneration can be affected by more than just cancer. In muscle atrophy, the balance between synthesis of new proteins and degradation of existing proteins is tipped towards the latter.[39] Atrophy in myotubes was induced by expressing ubiquitin ligase muscle atrophy F-box (MAFbx) in a rodent model.[40] Consistent with this observation, mice deficient in either ubiquitin ligase MAFbx or Muscle RING Finger 1 (MuRF1) were resistant to atrophy.[40] Besides degradation of proteins via the ubiquitin proteasome degradation pathway, the autophagy lysosomal degradation pathway is similarly important in skeletal muscles.[41] Both protein degradation pathways are controlled by Forkhead box protein O3 (FoxO3).[42]

Our study focused on cachexia where altered regeneration plays an important role in muscle wasting associated with cancer. We quantified a clear proteomic difference in muscle between cca and all other cohorts, some of which are affected by disease (cancer), others are healthy elderly (>75 years), and some of which show low RSMI. Our findings demonstrate that conventional weight loss measurements could be replaced by protein quantification with potential for early disease detection as seen by the heat map clustering (*Figure* 2B). Following these initial findings, we supported the identified protein signature by *in vitro* model system differentiating myoblasts of an 83-year-old donor into myofibres, a process interrupted by a single cytokine TNFα. Tumor necrosis factor α impairs myogenesis on multiple levels: from altering protein expression patterns of vital muscle regenerative proteins, e.g. MMP-14, over interference with FAK signaling pathway effecting actin-cofilin tube formation to dysregulated ATP synthase complex when compared with untreated myofibres. Hence, we are confident that a robust protein signature based on proteins belonging to the Fo complex, electron transport chain, and contractile fibre will be identified in follow-up studies comprised of more patient samples.

Acknowledgements

This work was supported by a Transfer Project grant from SystemsX.ch, The Swiss Initiative in Systems Biology.

Author contributions

H.A.E. and C.J. conceived the work. H.A.E., S.D., V.T., A.S., K.C. H.F., N.J., and C.A.G. collected data. H.A.E., C.J., and K.C.H.F. analysed and interpreted data. H.A.E. and C.J. drafted the manuscript. H.A.E., N.J., C.A.G., K.C.H.F., R.A., and CJ critically

revised the manuscript. All authors read and approved the submitted manuscript. Also, the authors certify that they comply with the ethical guidelines for publishing in the Journal of Cachexia, Sarcopenia, and Muscle: update 2015.[43]

Online supplementary material

Additional Supporting Information may be found in the online version of this article at the publisher's web-site:

Supporting Information Supplementary Data 1-mapDIA
Supporting Information Supplementary Data-89_prot_sig
Supporting Information Supplementary Data-hsadd04510_frames.gif
Supporting Information Supplementary-p-P38.pdf
Supporting Information peptide cleanup
Supporting Information SWATH data analysis
Supporting Information Supplementary-Abbreviations
Proteome data set: http://massive.ucsd.edu/ProteoSAFe/status.jsp?task=ba010a5598294233a28638e886446477

Conflict of interest

The authors declare that they have no conflict of interest.

References

1. Zammit PS, Partridge TA, Yablonka-Reuveni Z. The skeletal muscle satellite cell: the stem cell that came in from the cold. *The journal of histochemistry and cytochemistry: official journal of the Histochemistry Society* 2006;**54**:1177–1191.
2. Bowen TS, Schuler G, Adams V. Skeletal muscle wasting in cachexia and sarcopenia: molecular pathophysiology and impact of exercise training. *J Cachexia Sarcopenia Muscle.* 2015;**6**:197–207.
3. Argiles JM, Campos N, Lopez-Pedrosa JM, Rueda R, Rodriguez-Manas L. Skeletal muscle regulates metabolism via interorgan crosstalk: roles in health and disease. *J Am Med Dir Assoc* 2016;doi:10.1016/j.jamda.2016.04.019.
4. Kelley DE, He J, Menshikova EV, Ritov VB. Dysfunction of mitochondria in human skeletal muscle in type 2 diabetes. *Diabetes* 2002;**51**:2944–2950.
5. Cartee GD, Hepple RT, Bamman MM, Zierath JR. Exercise promotes healthy aging of skeletal muscle. *Cell Metab* 2016;**23**:1034–1047.
6. Macaluso A, De Vito G. Muscle strength, power and adaptations to resistance training in older people. *Eur J Appl Physiol* 2004;**91**:450–472.
7. Mitchell WK, Williams J, Atherton P, Larvin M, Lund J, Narici M. Sarcopenia, dynapenia, and the impact of advancing age on human skeletal muscle size and strength; a quantitative review. *Front Physiol* 2012;**3**:260, doi:10.3389/fphys.2012.00260.
8. Evans WJ, Morley JE, Argiles J, Bales C, Baracos V, Guttridge D, *et al.* Cachexia: a new definition. *Clin Nutr* 2008;**27**:793–799.
9. Fearon KC. Cancer cachexia: developing multimodal therapy for a multidimensional problem. *Eur J Cancer* 2008;**44**:1124–1132,.
10. Fearon KC, Voss AC, Hustead DS. Cancer Cachexia Study G. Definition of cancer cachexia: effect of weight loss, reduced food intake, and systemic inflammation on functional status and prognosis. *Am J Clin Nutr* 2006;**83**:1345–1350.
11. Cruz-Jentoft AJ, Baeyens JP, Bauer JM, Boirie Y, Cederholm T, Landi F, *et al.* Sarcopenia: European consensus on definition and diagnosis: Report of the European Working Group on Sarcopenia in Older People. *Age Ageing* 2010;**39**:412–423.
12. Gallagher D, Ruts E, Visser M, Heshka S, Baumgartner RN, Wang J, *et al.* Weight stability masks sarcopenia in elderly men and women. *Am J Physiol Endocrinol Metab* 2000;**279**:E366–E375.
13. Gallagher IJ, Jacobi C, Tardif N, Rooyackers O, Fearon K. Omics/systems biology and cancer cachexia. *Semin Cell Dev Biol* 2016;**54**:92–103.
14. Annesley TM. Ion suppression in mass spectrometry. *Clin Chem* 2003;**49**:1041–1044.
15. Parker KC, Walsh RJ, Salajegheh M, Amato AA, Krastins B, Sarracino DA, *et al.* Characterization of human skeletal muscle biopsy samples using shotgun proteomics. *J Proteome Res* 2009;**8**:3265–3277, doi:10.1021/pr800873q.
16. Hojlund K, Yi Z, Hwang H, Bowen B, Lefort N, Flynn CR, *et al.* Characterization of the human skeletal muscle proteome by one-dimensional gel electrophoresis and HPLC-ESI-MS/MS. *Mol Cell Proteomics* 2008;**7**:257–267.
17. Deshmukh AS, Murgia M, Nagaraj N, Treebak JT, Cox J, Mann M. Deep proteomics of mouse skeletal muscle enables quantitation of protein isoforms, metabolic pathways, and transcription factors. *Mol Cell Proteomics* 2015;**14**:841–853.
18. Murgia M, Nagaraj N, Deshmukh AS, Zeiler M, Cancellara P, Moretti I, *et al.* Single muscle fiber proteomics reveals unexpected mitochondrial specialization. *EMBO Rep* 2015;**16**:387–395.
19. Brocca L, Cannavino J, Coletto L, Biolo G, Sandri M, Bottinelli R, *et al.* The time course of the adaptations of human muscle proteome to bed rest and the underlying mechanisms. *J Physiol* 2012;**590**:5211–5230.
20. Staunton L, Zweyer M, Swandulla D, Ohlendieck K. Mass spectrometry-based proteomic analysis of middle-aged vs. aged vastus lateralis reveals increased levels of carbonic anhydrase isoform 3 in senescent human skeletal muscle. *Int J Mol Med* 2012;**30**:723–733.
21. Doran P, Donoghue P, O'Connell K, Gannon J, Ohlendieck K. Proteomics of skeletal muscle aging. *Proteomics* 2009;**9**:989–1003.
22. Doran P, Martin G, Dowling P, Jockusch H, Ohlendieck K. Proteome analysis of the dystrophin-deficient MDX diaphragm reveals a drastic increase in the heat shock protein cvHSP. *Proteomics* 2006;**6**:4610–4621.
23. Gillet LC, Navarro P, Tate S, Rost H, Selevsek N, Reiter L, *et al.* Targeted data extraction of the MS/MS spectra generated by data-independent acquisition: a new concept for consistent and accurate proteome analysis. *Mol Cell Proteomics* 2012;**11**: doi:10.1074/mcp.O111.016717.O111 016717
24. Greig CA, Young A, Skelton DA, Pippet E, Butler FM, Mahmud SM. Exercise studies with elderly volunteers. *Age Ageing* 1994;**23**:185–189.
25. Baumgartner RN, Koehler KM, Gallagher D, Romero L, Heymsfield SB, Ross RR, *et al.* Epidemiology of sarcopenia among the elderly in New Mexico. *Am J Epidemiol* 1998;**147**:755–763.
26. Schubert OT, Gillet LC, Collins BC, Navarro P, Rosenberger G, Wolski WE, *et al.* Building high-quality assay libraries for targeted analysis of SWATH MS data. *Nat Protoc* 2015;**10**:426–441.
27. Rosenberger G, Koh CC, Guo T, Röst HL, Kouvonen P, Collins BC, *et al.* A repository of assays to quantify 10,000 human proteins by SWATH-MS. *Scientific Data* 2014;**1**:doi:10.1038/sdata.2014.31 .http://www.nature.com/articles/sdata201431#supplementary-information
28. Rost HL, Rosenberger G, Navarro P, Gillet L, Miladinovic SM, Schubert OT, *et al.* OpenSWATH enables automated, targeted

analysis of data-independent acquisition MS data. *Nat Biotechnol* 2014;**32**: 219–223.
29. Rosenberger G, Ludwig C, Rost HL, Aebersold R, Malmstrom L. aLFQ: an R-package for estimating absolute protein quantities from label-free LC–MS/MS proteomics data. *Bioinformatics* 2014;**30**: 2511–2513.
30. Teo G, Kim S, Tsou CC, Collins B, Gingras AC, Nesvizhskii AI, *et al.* mapDIA: preprocessing and statistical analysis of quantitative proteomics data from data independent acquisition mass spectrometry. *J Proteomics* 2015;**129**:108–120.
31. Szklarczyk D, Franceschini A, Wyder S, Forslund K, Heller D, Huerta-Cepas J, *et al.* STRING v10: protein–protein interaction networks, integrated over the tree of life. *Nucleic Acids Res* 2015;**43**:D447–D452, doi:10.1093/nar/gku1003.
32. Dahlman I, Mejhert N, Linder K, Agustsson T, Mutch DM, Kulyte A, *et al.* Adipose tissue pathways involved in weight loss of cancer cachexia. *Br J Cancer* 2010;**102**:1541–1548.
33. Snyman C, Niesler CU. MMP-14 in skeletal muscle repair. *J Muscle Res Cell Motil* 2015;**36**:215–225, doi:10.1007/s10974-015-9414-4.
34. Henningsen J, Rigbolt KT, Blagoev B, Pedersen BK, Kratchmarova I. Dynamics of the skeletal muscle secretome during myoblast differentiation. *Mol Cell Proteomics* 2010;**9**:2482–2496.
35. Mizuno K. Signaling mechanisms and functional roles of cofilin phosphorylation and dephosphorylation. *Cell Signal* 2013;**25**:457–469.
36. Remels AH, Gosker HR, Schrauwen P, Hommelberg PP, Sliwinski P, Polkey M, *et al.* TNF-alpha impairs regulation of muscle oxidative phenotype: implications for cachexia? *FASEB journal: official publication of the Federation of American Societies for Experimental Biology* 2010;**24**:5052–5062.
37. Ebhardt HA, Root A, Sander C, Aebersold R. Applications of targeted proteomics in systems biology and translational medicine. *Proteomics* 2015;**15**:3193–3208.
38. Fukawa T, Yan-Jiang BC, Min-Wen JC, Jun-Hao ET, Huang D, Qian CN, *et al.* Excessive fatty acid oxidation induces muscle atrophy in cancer cachexia. *Nat Med* 2016;**22**:666–671.
39. Jagoe RT, Goldberg AL. What do we really know about the ubiquitin–proteasome pathway in muscle atrophy? *Curr Opin Clin Nutr Metab Care* 2001;**4**:183–190.
40. Bodine SC, Latres E, Baumhueter S, Lai VK, Nunez L, Clarke BA, *et al.* Identification of ubiquitin ligases required for skeletal muscle atrophy. *Science* 2001;**294**: 1704–1708.
41. Masiero E, Agatea L, Mammucari C, Blaauw B, Loro E, Komatsu M, *et al*. Autophagy is required to maintain muscle mass. *Cell Metab* 2009;**10**:507–515.
42. Mammucari C, Milan G, Romanello V, Masiero E, Rudolf R, Del Piccolo P, *et al*. FoxO3 controls autophagy in skeletal muscle in vivo. *Cell Metab* 2007;**6**:458–471.
43. von Haehling S, Morley JE, Coats AJ, Anker SD. Ethical guidelines for publishing in the Journal of Cachexia, Sarcopenia and Muscle: update 2015. *J Cachexia Sarcopenia Muscle* 2015;**6**:315–316.